Journal of Computational Physics **162,** 104–122 (2000)
doi:10.1006/jcph.2000.6527, available online at http://www.idealibrary.com on IDEAL®

A Level-Set Method for Simulating Island Coarsening

D. L. Chopp[1]

Engineering Sciences and Applied Mathematics Dept., Northwestern University, Evanston, Illinois 60208
E-mail: chopp@nwu.edu

Received December 23, 1996; revised August 5, 1997

Modeling of microstructural evolution during thin-film deposition requires a knowledge of several key activation energies (surface diffusion, island edge atom diffusion, adatom migration over descending step edges, etc.). These and other parameters must be known as a function of crystal orientation. In order to generate values for these parameters, we have developed a numerical simulation in tandem with physical experiments. By tuning the simulation to the results from experiments we can extract and verify approximate values for these parameters. The numerical method we use is based upon the level set method. Our model is a continuum model in directions parallel to the crystal facet, and resolves each discrete atomic layer in the normal direction. The model includes surface diffusion, step edge dynamics, and attachment/detachment rates all of which may depend upon the local geometry of the step edge. The velocity field for advancing the island edges in the level set framework is generated by computing the equilibrium adatom density on the flat terraces resulting in Laplace's equation with mixed boundary conditions at the step edges. We have turned to the finite element method for solving this equation, which results in very good agreement with analytically known solutions and with experiment.

1. INTRODUCTION

Modeling of microstructural evolution during thin-film deposition requires knowledge of several key activation energies (surface diffusion, island edge atom diffusion, adatom migration over descending step edges, etc.). These and other parameters must be known as a function of orientation. In order to generate values for these parameters, we have developed a numerical simulation in tandem with physical experiments. By tuning the simulation to results from experiments we can extract and verify approximate values for these parameters.

[1] Supported by the NSF/DARPA VIP program under Award 96-15877.

0021-9991/00 $35.00

The physical experiments to which we compare are the annealing of a very flat, about 10 atomic layers variation, sample of TiN. This material is often used, for example, as a diffusion barrier in semiconductor manufacturing. By studying the decay rate of various islands and voids in different initial configurations on the surface, we can extract the key activation energies by matching experiment to computed solutions of the mathematical model. By tuning the parameters, we get the mathematical model to agree with the experiment and thereby deduce the value of the different parameters. While we are using TiN, this procedure could be repeated for a wide variety of important materials provided the availability of experimental data.

The numerical method we use is based upon the level set method. Our model is a continuum model in directions parallel to the crystal facet, and resolves each discrete atomic layer in the normal direction. The model includes surface diffusion, step edge dynamics, and attachment/detachment rates all of which may depend upon the local geometry of the step edge.

The velocity field for advancing the island edges in the level set framework is generated by computing the equilibrium adatom density on the flat terraces resulting in Laplace's equation with mixed boundary conditions at the step edges. The step edge velocity is then derived from the normal derivative of the adatom density. Thus, it is important that we achieve accurate approximations for the adatom density up to the step edges. To achieve this accuracy we have turned to a finite element method for solving the elliptic equation. This results in very good agreement with analytically known solutions. This gives us confidence that the derived value of the material parameters will have reasonable accuracy.

In this paper we present the details of the numerical aspects of this project. In Section 2, we discuss previous work in this area. In Section 3, we present an overview of the physical experiment and describe the mathematical model we will be using to simulate the experimental conditions. In Section 4, we give an overview of our numerical method including brief overviews of the level set and finite element methods. In Section 5, we demonstrate the accuracy of our method and give example comparisons between simulation and experiment. The work of extracting all the physical parameters using this simulation is in progress and will be reported elsewhere.

2. BACKGROUND

Modeling the relaxation of atomic scale features of small islands and clusters of islands on the surface of a condensed phase of material has been the subject of research for many years. However, it was not until the arrival of atomic scale microscopy that it became possible to study and analyze the behavior of individual islands and the interaction of islands. The analysis at this level will lead to improvements in the study of, for example, deposition, epitaxial growth, and sintering.

Much of the analysis in this area derives from the study of Ostwald ripening. Overviews of the research of Ostwald ripening and island dynamics can be found in the review articles [45, 47]. Early work on diffusion processes in the context of Ostwald ripening include for example [8, 15, 22]. The focus of attention on individual mono-atomic islands and their interaction is more recent. Experimental investigations of adatom island migration and diffusion can be found in [12, 31, 43] and analysis and simulation can be found in [7, 20, 24, 39, 27]. Experimental investigations into step-edge motion and adatom island decay can

be found in, for example, [5, 13, 17, 18, 26, 32, 40, 43]. Analysis and simulation of island decay can be found in [25, 44, 48].

The rate of decay or growth of individual islands during annealing is often dominated by one of two different rate-limiting steps. For diffusion-limited kinetics, adatoms are able to attach and detach from step edges easily compared with their rate of diffusion on the terraces. This leads to, for example, larger adatom densities around convex islands. For detachment-limited kinetics, the rate-limiting step is the formation energy required for an adatom to detach from a step edge. In this regime, the adatoms, once they detach, very quickly locate a new attachment site. This leads to a low, nearly constant, adatom density on the terraces.

One way the two regimes can be distinguished experimentally is by the growth and decay of individual islands within a cluster. For diffusion-limited kinetics, there is greater dependence on the surrounding island configuration due to the large variation in the local adatom density. This can be observed experimentally by noticing that large islands exhibit "denuding zones" where small islands neighboring a large island decay more rapidly than those of the same initial size further away. Denuded zones have been observed, for example, in [28]. Detachment-limited kinetics, by contrast, results in more localized decay rates independent of the surrounding island configuration.

The class of materials that we are investigating assume diffusion-limited kinetics. Materials observed to exhibit diffusion-limited kinetics include copper (111) [14], silver (111) [26], and titanium nitride (002) [19]. Materials observed to exhibit detachment-limited kinetics include gold (111) [32], copper (100) [18], copper (001) [17], and silicon (001) [6].

Our model also includes the Ehrlich step edge barrier. The Ehrlich barrier at step edges is based on the observation that the energy required to go over the step edge is greater than the energy required to jump to a different site on the same terrace. It was observed experimentally by Ehrlich and Hudda [11] and also studied by Schwoebel and Shipsey [33]. The barrier explains that it is less probable that an adatom will go down the step than to remain on the same terrace, and even less likely for an adatom to go up a step to a higher terrace. Figure 1, an illustration similar to that found in [33] illustrates the adatom potential energy function and the Ehrlich barrier. The strength of the Ehrlich barrier is key

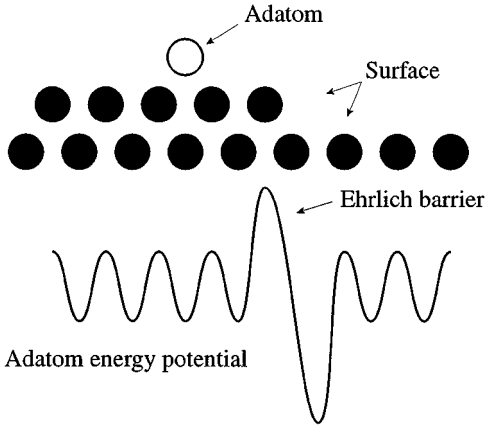

FIG. 1. Illustration of the adatom potential function and the Ehrlich barrier.

to predicting the surface roughness during deposition. Evidence of the importance of the Ehrlich barrier in the model can be found, for example, in [26].

Numerical simulations of island motion and decay include using a modified meanfield theory [6], a nearest neighbor island interaction model [27], kinetic Monte Carlo [40, 28, 24, 25], molecular dynamics [20], and level sets [16].

The algorithm presented here is capable of modelling much more complex initial island configurations, as seen experimentally, than the non-level set methods mentioned above. Initializing the method requires only an STM image and a few minutes using the public domain NIH image program [29] to color the different atomic layer heights.

For example, in [27], Morgenstern *et al.* are able to model multiple islands and produce very good qualitative comparisons to experiment, but they admit that matching to experiment would be difficult because the construction of the flux functions results in a consistent underestimate for the flux and must be compensated for by overestimating the diffusion rate. This makes their method unsuitable for the parameter estimation task before us. They also note that mean-field theory is inadequate for predicting island decay rates. The method presented here is not based on mean-field theory; instead a more complete flux function is constructed which produces a more accurate representation of the flux over the length of the step edges.

There are some key distinctions between the method presented here and the approach used in [16]. First, the representation of the islands is done with level set functions for each atomic layer as opposed to a single level set function as in [16]. While there is some additional cost due to the multiple level sets, it is offset by the greater accuracy of the representation and the edge velocities when multiple step edges at different heights are close together. Second, and most important, the use of level sets coupled with finite elements is a way to more accurately compute the adatom density on the terraces resulting in improved approximations for the step edge velocity.

The coupling of level sets and finite elements in this way is a relatively new approach with much potential beyond the current application. A simple example where it has been applied is in mechanical stress calculations as found in [42] and is being extended to solve problems of crack propagation in solids.

3. MATHEMATICAL MODEL

Elements of the model we use for our simulation can be found in the analyses of Villain [44], Zinke-Allmang *et al.* [48], and McLean *et al.* [25] which in turn rely on the Lifshitz-Slyozov theory [22]. For this simulation we assume the process is in the diffusion-limited regime, meaning that the rate-limiting step in the diffusion process is due to the diffusion of adatoms on the open terraces. However, the diffusion process is fast enough that we can assume the adatom density on the terraces is always near equilibrium. Since there is no deposition of atoms onto or evaporation of atoms off of the surface, there are no sources or sinks on the open terraces away from step edges. Therefore, the equilibrium adatom density on the terraces is determined by Laplace's equation,

$$\Delta\rho = 0.$$

Furthermore, we assume that the adatom density at one terrace height is not influenced by the adatom density at other terrace heights. Thus, we decompose our computational domain into a collection of independent Laplace problems, one for each terrace bounded

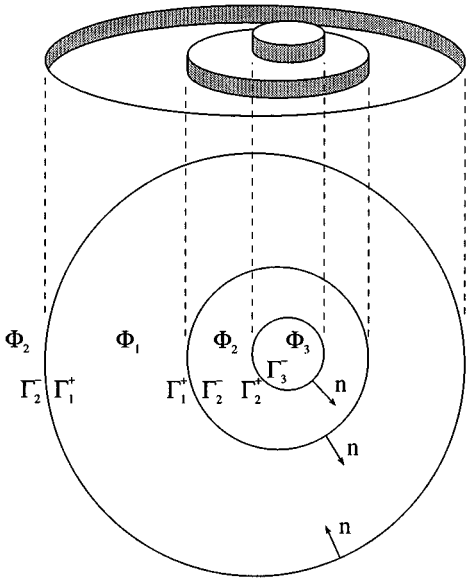

FIG. 2. Illustration of the decomposition of the domain.

by step edges. We illustrate this decomposition in Fig. 2. From here on we refer to a single connected terrace bounded by step edges as a terrace domain.

The flux of adatoms to and from a terrace domain occurs entirely at the step edges, leading to mixed boundary conditions at the step edges. There are two types of steps to demark the boundary of the domain: up steps and down steps. The boundary conditions for the Laplace equation are different depending upon which type of step.

For an up step, we refer to the analysis presented in [25] to get the up step boundary condition given by

$$D\frac{\partial \rho}{\partial n} = -K\left(\rho_r^{\mathrm{eq}} - \rho\right),$$

where D is the surface adatom diffusion rate, K is the adatom attachment rate, and

$$\rho_r^{\mathrm{eq}} = \rho_\infty^{\mathrm{eq}} \exp\left(\frac{\gamma\Omega}{kTr}\right), \tag{1}$$

as given by the Gibbs–Thompson relation. Here, n is the normal to the terrace domain at the step edge pointing towards the lower terrace level (see Fig. 2), r is the local radius of curvature ($r > 0$ for convex step edge), γ is the line tension, Ω is the surface area covered by a single diffusing species, k is the Boltzmann constant, and T is the temperature of the simulation. The constant $\rho_\infty^{\mathrm{eq}}$, as given in [25], is the adatom density at a straight step edge ($r = \pm\infty$). The values of D and $\rho_\infty^{\mathrm{eq}}$ in turn depend on the annealing temperature by the relations

$$D = D_0 \exp\left(\frac{-E_d}{kT}\right) \quad \rho_\infty^{\mathrm{eq}} = C_0 \exp\left(\frac{-E_f}{kT}\right),$$

where E_d is the surface diffusion barrier and E_f is the adatom formation energy.

For a down step, we assume the presence of an Ehrlich barrier which inhibits adatoms from stepping down to the next atomic layer. While this barrier is not strong, it can play a role in the microstructural evolution, so we include it in our model. We assume that a certain fraction of the adatoms approaching a step edge successfully overcome the barrier and go down to the next lower terrace level and attach to the step edge. Therefore, we get a boundary condition for the down steps to be

$$D\frac{\partial \rho}{\partial n} = -\alpha\rho$$

where α is the fraction of adatoms that will successfully overcome the barrier.

Note that we have set the equilibrium adatom density at the down step to be zero. This is consistent with the conventional form of the diffusion barrier (see Fig. 1) where there is no assumed retention of adatoms at the top of a down step. It is observed in [21] that the actual condition at the down step may be more complicated, and there can be some retention of adatoms at the top of down steps of some materials. Adding this feature to the model would change the down step boundary condition to

$$D\frac{\partial \rho}{\partial n} = \alpha(\tilde{\rho}^{\mathrm{eq}} - \rho)$$

where $\tilde{\rho}^{\mathrm{eq}}$ would be the equilibrium density of adatoms at the top of step edges. The algorithm presented here can easily be modified to incorporate this change.

Note also that for a free adatom on one terrace to migrate to the next lower terrace and become a free adatom on the terrace below, it must first overcome the Ehrlich barrier and attach to the lower step edge before it can detach from the lower step edge; this allows us to say that the different adatom density calculations are decoupled.

Finally, the boundary conditions at the edges of the computational domain are taken to be no-flux conditions; i.e., $\partial\rho/\partial n = 0$ at the boundary, where n is normal to the boundary. This is equivalent to assuming that the island configuration is a mirror image on each side of the rectangular domain. While this limits the accuracy of the behavior near the edges of the domain, it is observed in [27] that the growth/decay rates of islands depends most heavily upon the local geometric configuration under diffusion limited conditions. This means that the results in the interior of the domain should remain valid despite the imperfect approximation at the edges.

Putting this all together, for any given single terrace domain Φ, we decompose the boundary Γ of Φ into two parts, Γ^+ and Γ^-, where Γ^+ is the boundary consisting of up steps and Γ^- is the boundary consisting of down steps. Therefore, for each exposed terrace level, we must solve

$$\Delta\rho(x) = 0, \quad x \in \Phi \tag{2}$$

$$D\frac{\partial \rho}{\partial n} = -K\left(\rho_r^{\mathrm{eq}} - \rho\right), \quad x \in \Gamma^+ \tag{3}$$

$$D\frac{\partial \rho}{\partial n} = -\alpha\rho, \quad x \in \Gamma^-. \tag{4}$$

We illustrate this construction in Fig. 2.

Finally, given a point x at a step edge, we need to know the net flux of adatoms at x. The net flux, i.e., the normal speed F of the step edge in the direction of the normal, is given by

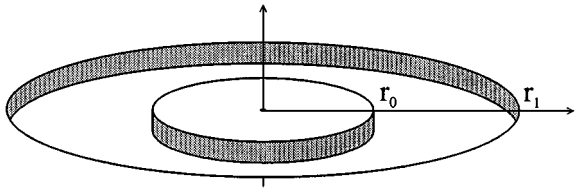

FIG. 3. Island in a pit configuration.

the sum of the flux from below and above; thus

$$F(x) = -D\left(\frac{\partial \rho^-}{\partial n}(x) + \frac{\partial \rho^+}{\partial n}(x)\right), \tag{5}$$

$$= K\left(\rho_r^{\mathrm{eq}}(x) - \rho^-(x)\right) + \alpha\rho^+(x) \tag{6}$$

where the $+$ indicates the adatom density on the upper side of the step edge and the $-$ indicates the adatom density of the lower side of the step edge. We will use this normal velocity to evolve the level set method as described in Section 4.

3.1. *Special Case: Island in a Pit*

To test the accuracy of our numerical method against the model, we will compare our computed solution with some special cases. The first special case is a circular island located in the center of a circular pit. Suppose the center island has radius r_0 and the pit has radius r_1, as illustrated in Fig. 3. Since this is a rotationally symmetric problem, we can reduce the dimension of our problem to one dimension and it is given by the three boundary value problems

$$\begin{gathered}\rho''(r) + \frac{1}{r}\rho'(r) = 0, \quad r_0 < r < r_1 \\ D\rho'(r_0) = -K\left(\rho_{r_0}^{\mathrm{eq}} - \rho(r_0)\right), \quad D\rho'(r_1) = K\left(\rho_{r_1}^{\mathrm{eq}} - \rho(r_1)\right)\end{gathered} \tag{7}$$

$$\begin{gathered}\rho''(r) + \frac{1}{r}\rho'(r) = 0, \quad 0 < r < r_0 \\ D\rho'(r_0) = -\alpha\rho(r_0), \quad \rho'(r=0) = 0\end{gathered} \tag{8}$$

$$\begin{gathered}\rho''(r) + \frac{1}{r}\rho'(r) = 0, \quad r > r_1 \\ D\rho'(r_1) = \alpha\rho(r_1), \quad \lim_{r\to+\infty} D\rho'(r) = 0\end{gathered} \tag{9}$$

Note that the radius of curvature in the boundary condition of Eq. (7) at $r = r_1$ is taken to be negative because the terrace edge is concave. It is easy to see that Eqs. (8) and (9) are uniquely solved by $\rho(r) \equiv 0$, and hence do not contribute to the motion of the step edge. We therefore turn our attention to Eq. (7).

We can solve Eq. (7) explicitly to get

$$\begin{aligned}\rho(r) = {} & \rho_\infty^{\mathrm{eq}}(D(r_1 + r_0) + Kr_0r_1\ln(r_1/r_0))^{-1} \\ & \times \left((Dr_0 + Kr_0r_1\ln(r_1) - Kr_0r_1\ln(r))\exp\left(\frac{\gamma\Omega}{kTr_0}\right)\right. \\ & \left. + (Dr_1 - Kr_0r_1\ln(r_0) + Kr_0r_1\ln(r))\exp\left(\frac{-\gamma\Omega}{kTr_1}\right)\right).\end{aligned} \tag{10}$$

Plugging this solution into Eq. (5) for $r = r_0, r_1$ yields a pair of coupled ordinary differential equations for the motion of the step edges located at r_0 and r_1,

$$r_0'(t) = \frac{-DK\rho_\infty^{\mathrm{eq}}(\exp(\gamma\Omega/kTr_0(t)) - \exp(-\gamma\Omega/kTr_1(t)))r_1(t)}{D(r_0(t)+r_1(t)) + Kr_0(t)r_1(t)\ln(r_1(t)/r_0(t))} \tag{11}$$

$$r_1'(t) = \frac{-DK\rho_\infty^{\mathrm{eq}}(\exp(\gamma\Omega/kTr_0(t)) - \exp(-\gamma\Omega/kTr_1(t)))r_0(t)}{D(r_0(t)+r_1(t)) + Kr_0(t)r_1(t)\ln(r_1(t)/r_0(t))}. \tag{12}$$

We can solve these equations numerically to arbitrary accuracy using a standard adaptive Runge–Kutta ODE solver. Plots of these solutions are provided in Section 5.

3.2. *Special Case: Three Stacked Islands*

While the first test case is commonly used to derive some of the physical parameters from experiment, it does not include a non-trivial use of the Ehrlich barrier parameter. To test this part of our method and also to test the summing present in Eq. (5), we turn to a different initial configuration. In this configuration we have three concentric stacked islands as depicted in Fig. 4. Let r_0, r_1, r_2 be the radii of the top, middle, and bottom islands, respectively. We must therefore solve four different Laplace equations

$$\begin{gathered}\rho''(r) + \frac{1}{r}\rho'(r) = 0, \quad 0 < r < r_0 \\ D\rho'(r_0) = -\alpha\rho(r_0), \quad D\rho'(0) = 0\end{gathered} \tag{13}$$

$$\begin{gathered}\rho''(r) + \frac{1}{r}\rho(r) = 0, \quad r_0 < r < r_1 \\ D\rho'(r_0) = -K\left(\rho_{r_0}^{\mathrm{eq}} - \rho(r_0)\right), \quad D\rho'(r_1) = -\alpha\rho(r_1)\end{gathered} \tag{14}$$

$$\begin{gathered}\rho''(r) + \frac{1}{r}\rho'(r) = 0, \quad r_1 < r < r_2 \\ D\rho'(r_1) = -K\left(\rho_{r_1}^{\mathrm{eq}} - \rho(r_1)\right), \quad D\rho'(r_2) = -\alpha\rho(r_2)\end{gathered} \tag{15}$$

$$\begin{gathered}\rho''(r) + \frac{1}{r}\rho'(r) = 0, \quad r_2 < r \\ D\rho'(r_2) = -K\left(\rho_{r_2}^{\mathrm{eq}} - \rho(r_2)\right), \quad \lim_{r\to+\infty} D\rho'(r) = 0.\end{gathered} \tag{16}$$

As in the previous special case, Eqs. (13), (16) have trivial solutions given by $\rho(r) \equiv 0$ and $\rho(r) \equiv \rho_\infty^{\mathrm{eq}} \exp(\gamma\Omega/kTr_2)$, respectively, leaving $\rho'(r) \equiv 0$ in both cases, and hence they do not contribute to the motion of the step edges.

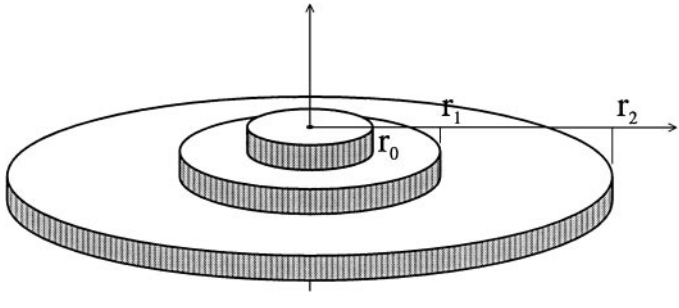

FIG. 4. Three concentric stacked islands configuration.

The solutions for Eqs. (14) and (15) are the same up to certain indices, so we will just discuss Eq. (14). The solution for (14) is given by

$$\rho(r) = \frac{Kr_0\rho_\infty^{\text{eq}} \exp(\gamma\Omega/kTr_0)\,(D + \alpha r_1(\ln(r_1) - \ln(r)))}{D\alpha r_1 + DKr_0 + K\alpha r_0 r_1 \ln(r_1/r_0)} \tag{17}$$

Plugging this into Eq. (5) will contribute to the motion of edges located at r_0 and r_1.

If we combine both the solutions for Eqs. (14) and (15) into Eq. (5), we again get a system of ordinary differential equations for the motion of the radii r_0, r_1, and r_2:

$$r_0'(t) = \frac{-DK\alpha r_1(t)\rho_\infty^{\text{eq}} \exp(\gamma\Omega/kTr_0(t))}{D\alpha r_1(t) + DKr_0(t) + \alpha Kr_0(t)r_1(t)\ln(r_1(t)/r_0(t))} \tag{18}$$

$$\begin{aligned} r_1'(t) = {} & \frac{DK\alpha r_0(t)\rho_\infty^{\text{eq}} \exp(\gamma\Omega/kTr_0(t))}{D\alpha r_1(t) + DKr_0(t) + \alpha Kr_0(t)r_1(t)\ln(r_1(t)/r_0(t))} \\ & - \frac{DK\alpha r_2(t)\rho_\infty^{\text{eq}} \exp(\gamma\Omega/kTr_1(t))}{D\alpha r_2(t) + DKr_1(t) + \alpha Kr_1(t)r_2(t)\ln(r_2(t)/r_1(t))} \end{aligned} \tag{19}$$

$$r_2'(t) = \frac{DK\alpha r_1(t)\rho_\infty^{\text{eq}} \exp(\gamma\Omega/kTr_1(t))}{D\alpha r_2(t) + DKr_1(t) + \alpha Kr_1(t)r_2(t)\ln(r_2(t)/r_1(t))}. \tag{20}$$

We can again solve this using a standard ODE solver to specified accuracy. Plots can be found in Section 5.

4. NUMERICAL METHOD

The numerical method we use to simulate annealing is a combination of the level set method for following the evolving step edges and the finite element method for computing the velocity. We have chosen this approach because of the requirement for accurate values of the adatom density function *at* the step edge, not just near it. We will show in Section 5 that this approach pays off, by comparing a computed solution using this method with the test cases described in the previous section. We give a brief description of each part of the method below, followed by how we have combined these methods.

4.1 *The Level Set Method*

One of the most versatile and effective ways of computing the motion of curves and surfaces is the level set methodology developed by Osher and Sethian [30]. The calculations and numerical methodologies introduced in [9, 30, 34, 36] have, in recent years, provided the basis for a large collection of calculations in such areas as combustion and fluid mechanics [46], medical imaging [23], material science [10], and etching and deposition in semiconductor manufacturing [1–3]. For a review and resource on level set methods, see [37].

In the level set approach, both the interface of interest and the interface velocity field are embedded in higher dimensional functions. The main advantages of a level set approach are that topological changes are handled naturally, the technique is unchanged in three and higher dimensions, and finite difference schemes can be used for approximating operators on a fixed Eulerian mesh.

Imagine a closed curve Γ in the plane propagating normal to itself with speed F. We can embed the initial position of the front as the zero level set of a higher dimensional function

ϕ, and then identify the evolution of this function ϕ with the propagation of the front itself through a time-dependent initial value problem. At any time, the front is given by the zero level set of the time-dependent level set function ϕ. In order to derive an equation of the motion for this level set function ϕ, we stipulate that the zero level set of the evolving function ϕ always match the propagating hyper-surface, which means that

$$\phi(x(t), t) = 0. \tag{21}$$

By the chain rule,

$$\phi_t + \nabla\phi(x(t), t) \cdot x'(t) = 0. \tag{22}$$

Since F supplies the speed in the outward normal direction, $x'(t) \cdot n = F$, where $n = \nabla\phi/\|\nabla\phi\|$, and this yields an evolution equation for ϕ, namely,

$$\begin{aligned} &\phi_t + F\|\nabla\phi\| = 0 \\ &\phi(x, t = 0) \text{ given.} \end{aligned} \tag{23}$$

This is the level set equation introduced by Osher and Sethian [30].

As analyzed by Sethian in [35], the efficient solution of these front propagation problems requires the use of upwind difference schemes and schemes borrowed from the solution of hyperbolic conservation laws. A detailed discussion of such schemes in the context of interface propagation schemes may be found in [37].

One of the drawbacks to the level set approach is its requirement that the speed function F be given in the entire domain of ϕ. This information is not always available. For example, in our discussion above, we generate the speed of the step edges on the step edge, but we do not want to rely on the gradient of the density function ρ to supply velocities in the rest of the domain because of numerical stability issues. Fortunately, there is a technique for taking a speed F known on the interface only and extending it in a reasonable way to the rest of the domain of ϕ. That technique is based upon the fast marching method described next.

4.2. *The Fast Marching Method*

In order for the level set method to be applied, the velocity field F itself must be defined on the entire domain of ϕ, not just the zero level set corresponding to the interface itself. We can be more precise by rewriting the level set equation as

$$\phi_t + F_{\text{ext}}\|\nabla\phi\| = 0 \tag{24}$$

where F_{ext} is some velocity field which, at the zero level set, equals the given speed F. In other words,

$$F_{\text{ext}} = F \quad \text{on} \quad \phi = 0.$$

This new velocity field F_{ext} is known as the "extension velocity."

In [4], a technique was introduced for building this extension velocity field F_{ext} from a velocity field given on the front in a highly efficient and accurate manner. This technique relied on the Fast Marching Method [38], which is the optimal technique for solving the Eikonal equation.

Briefly, the Fast Marching method solves an equation of the form

$$\|\nabla u\| = \frac{1}{G(x, y)} \tag{25}$$

by first replacing the gradient by suitable upwind operators and then systematically advancing the front by marching outwards from the boundary data in an upwind fashion. The key to the algorithm lies in the observation that an upwind operator implies a causality, and hence grid points with a given value for u cannot be affected by those with a bigger value. Hence, as the solution is advanced, we can maintain a heap sort which keeps track of the smallest element to be updated, and thus always advances the solution "downwind" of that point. Through the use of this sorting algorithm, each point in the domain is visited *only once*, rather than requiring any iteration; the resulting technique has a total operation count of $O(N \log N)$.

This technique is then used to construct the extension velocity F_{ext} by computing the signed distance function u (obtained by letting $G(x, y) = 1$ in Eq. (25)) while simultaneously solving the associated equation

$$\nabla F_{\text{ext}} \cdot \nabla u = 0. \tag{26}$$

The resulting velocity field F_{ext} equals the velocity on the front and is reasonably smooth off of the front.

4.3. *Finite Element Method*

To generate the velocity at the step edges, we must solve the elliptic equation (2). Ideally, we would solve this problem on the existing fixed mesh on which we are evolving the step edges, but this would only give values for the adatom density at points near the step edge, not on it. Using judicious applications of interpolation between mesh points, one can get approximations for the adatom density function at the step edge, but the accuracy of such attempts does not appear to be as good as is needed for advancing the level set contours.

For that reason we have turned to the finite element method to handle Eq. (2). It is a very well established and successful method for solving elliptic equations, and error estimates for the accuracy of solutions can be obtained. Furthermore, by placing nodes precisely where we need them to initialize the fast marching velocity extension method described above, we get good approximations for the adatom density function, and hence the speed function F necessary to drive the level set representation of the step edges as given by Eq. (5). For a more detailed description of the finite element method, there are many texts available on the subject; for example, see [41].

In our implementation of this method, we use a Galerkin method with linear triangular elements, and assumed linear variation of the boundary data. This gives us a sparse linear system which we solve using a conjugate gradient method. We solve all terrace domains with the same step height simultaneously, so we solve one such finite element system for each exposed atomic layer.

We now detail the connection between the finite element method mesh and the level set method. To illustrate this point, suppose we are solving the elliptic equation on a terrace domain Φ at step height ℓ_Φ which is bounded by step edges. The finite elements are constructed by decomposing the level set mesh into triangular elements. Consider a set of four mesh points from the level set mesh which are arranged in a square. If all four points

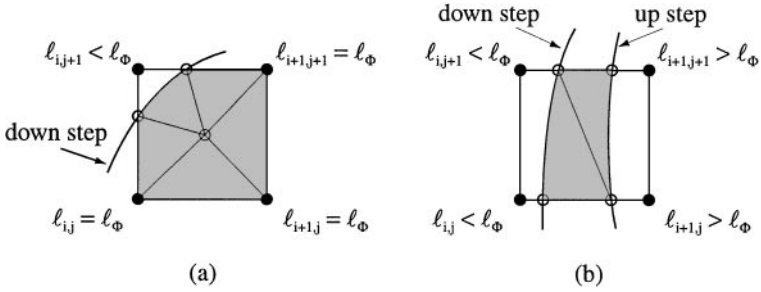

FIG. 5. Examples of finite element mesh construction.

are contained in Φ, then the square is cut in half down its diagonal into two triangles, each becoming a single finite element.

The difficult case is when one or more of the points lie outside Φ. Each mesh point is assigned the terrace level at that mesh point; call it ℓ_{ij}. There are three possibilities for each of the mesh points: (1) $\ell_{ij} < \ell_\Phi$, (2) $\ell_{ij} = \ell_\Phi$, (3) $\ell_{ij} > \ell_\Phi$. Three independent possibilities at each of four different mesh points leads to $3^4 = 81$ different cases and all but two (all case (1) or all case (3)) lead to one or more triangular elements. We illustrate these different cases with two examples.

As a simple example, suppose that three of the mesh points are in Φ, but the upper left node is not (see Fig. 5a). The best choice we found for this case is to place a node at the center of mass of the truncated square, and then form triangles from the center point out to each of the points on the perimeter as illustrated in Fig. 5a.

For an example of how multiple level sets can be useful, consider the case where the two left mesh points are lower than ℓ_Φ and the two right mesh points are higher, as in Fig. 5b. In this case, just because none of the mesh points are inside Φ does not mean that there are no elements to be included. In this case, the level set functions are used to locate the region which is at the correct height, between the left and the right. The resulting region is then triangulated into two triangles as illustrated. Here we see if a single level set function were used, we would not be able to pinpoint the location of each of the individual intermediate steps such as in this example. The other 77 cases which produce triangular elements are handled in a similar fashion. The boundary conditions for the domain are also incorporated in this process.

After the finite element mesh is constructed and the resulting linear system is solved, we are left with explicit values for the adatom density *on the interface*. No further interpolation is necessary to evaluate the flux at the boundary or to compute the resulting step edge velocity necessary for advancing the level set method. The computed velocity is then extended to the domain of the level set functions using the fast marching method as discussed above.

This type of finite-element implementation results in a first-order accurate solution. Higher order solutions are possible using higher order elements, but they come at a higher computational price. We found we get adequate accuracy using this method, as demonstrated by the test case solutions in Section 5.

4.4. *The Completed Algorithm*

We begin our description of the total algorithm with our representation of the step edges. In our implementation, we assign a single level set function ϕ_ℓ to each incomplete atomic layer ℓ. We illustrate the relationship between the ϕ_ℓ and the physical configuration in

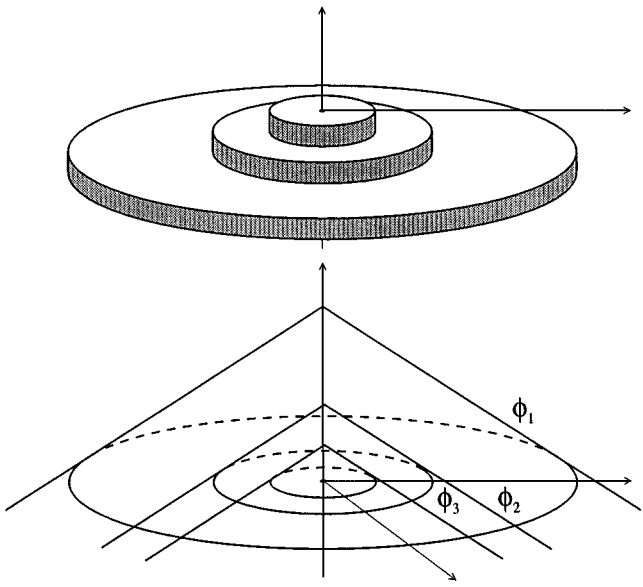

FIG. 6. Level set representation of single atomic layer islands.

Fig. 6. An island at atomic layer ℓ is present whenever $\phi_\ell(x) \geq 0$, and hence the step edge is given by $\{x : \phi_\ell(x) = 0\}$. While it is not necessary, it is generally the case that for a given x, $\phi_\ell(x) \geq \phi_{\ell+1}(x)$ indicating that there are no overhangs.

This approach differs from that in [16], where a single level set function is used to represent all atomic layers. We chose our approach instead because the level set method has better stability properties if the level set function itself does not have large variation in the gradient $\|\nabla\phi\|$. In fact, by using the velocity extension method described above, we can maintain $\|\nabla\phi\| \approx 1$ almost everywhere without costly reinitialization. Eliminating the need for reinitialization reduces computational cost and the amount of artificial diffusion generated by the numerical method.

Given the level set representation of the surface configuration, we next must construct the sequence of elliptic problems to be solved via the finite element method. We generate a single elliptic equation for each exposed atomic layer. The mesh generation for layer ℓ is done by passing through the mesh to look for all instances where the surface is at height ℓ, i.e. $\phi_\ell \geq 0 \geq \phi_{\ell+1}$. The boundary of the domain consists of the down steps Γ^- where $\phi_\ell = 0$ and also the up steps Γ^+ where $\phi_{\ell+1} = 0$. Every grid point in the mesh that is in the domain becomes a node as well as every intersection point between the boundary and grid lines. The entire domain is then triangulated using these nodes. For down steps, the Ehrlich barrier parameter α is a constant independent of the local geometry. For up steps, we use finite differences to compute an approximation to the local curvature κ of the boundary using the formula that can be found in [9], [10], or [30]. This value can then be inserted into the Gibbs–Thompson relation by

$$\exp\left(\frac{\gamma\Omega}{kTr}\right) = \exp\left(\frac{\gamma\Omega\kappa}{kT}\right),$$

where we have replaced the local radius of curvature r with the inverse of the curvature κ. We use the conjugate gradient method to solve the sparse linear systems, then use Eq. (5) to compute the speed of the step edges.

Now that we have the velocity of the step edge itself, we use the fast marching method to generate a velocity extension for each ϕ_ℓ which extends the step edge velocity outward to the rest of the domain of ϕ_ℓ. This velocity extension is generated in such a way that $\|\phi_\ell\| \approx 1$ is maintained. This ensures a stable calculation and eliminates the need for reinitialization. We use the extended velocity to advance ϕ_ℓ via the level set evolution Eq. (23) to complete a single time step.

It is easy to see from the exponential term in Eq. (1) that a relatively small island can result in some very large velocities at the step edge. This presents a problem in solving Eq. (2), and also in maintaining stability of the explicit level set method. We handle the first difficulty by placing a minimum value for the local radius of curvature to correspond to the diameter of a single adatom. Thus, the smallest representable island consists of a 2×2 atom square island.

The second problem is easily dealt with by using adaptive time stepping which is inversely proportional to the maximum computed velocity. Adaptive time stepping is almost necessary when we consider that in a typical calculation involving 30–50 islands, the ratio of the largest time step to the smallest is on the order of 10^6.

5. RESULTS

To demonstrate the accuracy of the method we have outlined above, we will compute solutions to the two model problems presented in Section 3. We will also compare our computed solution against a time sequence of images taken from an annealing experiment. By comparing well against both theory and experiment we will demonstrate that this method is a viable means of deriving the correct physical parameters for our model with the associated properties of the given material.

We begin with the comparison to known solutions of the mathematical model. In Fig. 7, we show a plot of the solution of the Island in a Pit model problem with a plot of our computed fully 2-dimensional solution. In the graph, we are comparing the total area of the

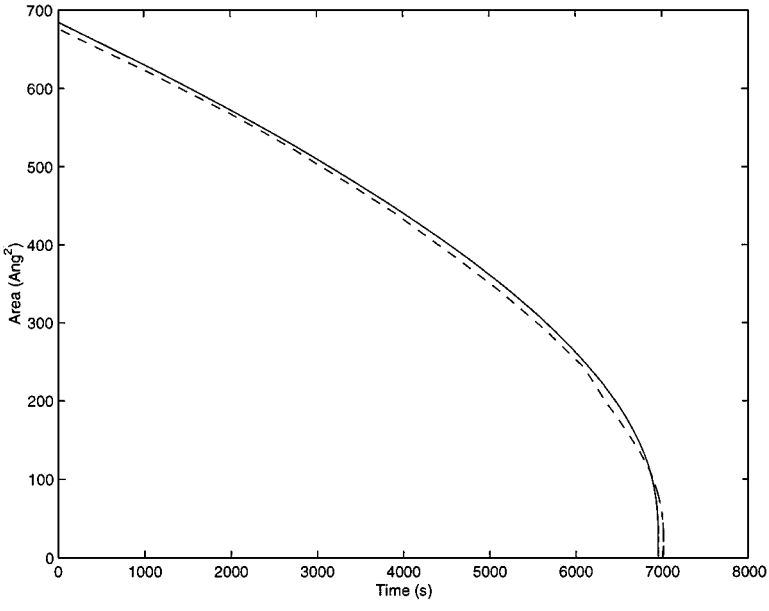

FIG. 7. Plot of full simulation vs ODE solution for island in a pit.

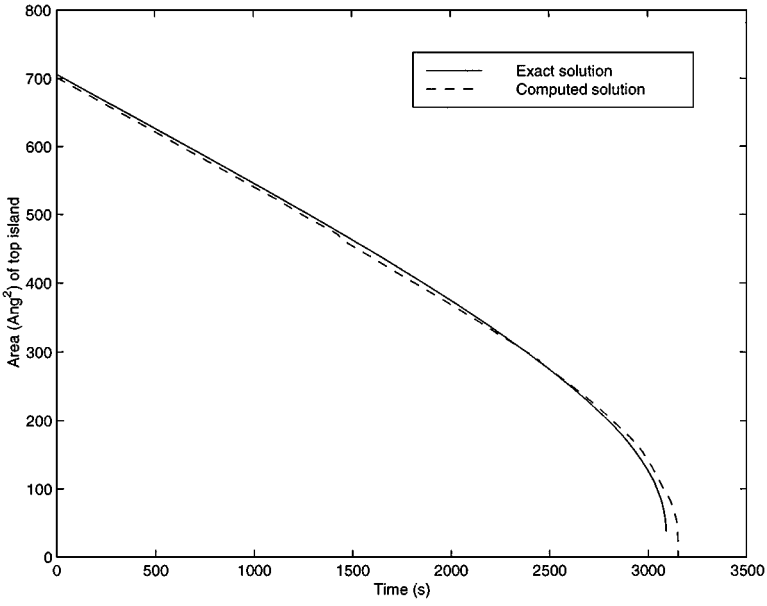

FIG. 8. Plot of full simulation vs ODE solution for top island.

center island as it decays in time. The computed solution does not quite decay fast enough in the final moments, but the overall agreement is very good, and we predict the time of the dissolution of the center island with less than 1% error. Note that for this calculation, we used parameter values of $D = 3.2959 \times 10^{-4}$, $K = 1$, $\rho_\infty^{\text{eq}} = 12.5825$, and $\alpha = 0.5$.

The previous comparison is not quite complete in that it only consists of up-step boundaries. None of the down-step boundaries contribute to the evolution as noted earlier. The next comparison combines both up-step and down-step boundaries. In this case, we have three concentric islands stacked on top of each other. The middle island step edge then gets non-zero contributions from both the up-step and down-step boundary conditions. In Figs. 8 and 9 we show the total area of each of the top and middle islands as they evolve. The top, smallest island decays, then dissolves. The middle island grows until the top island dissolves and then begins to decay. This time we predict the dissolution of the smallest island to less than 2% error. If we check for mass conservation of the method, the mass is preserved to within 0.07% error so we have very good mass conservation.

Finally, we take an image of initial experimental conditions and compare our predicted evolution of the islands with the experimental data. In Fig. 10 we show the experimental data in the left column and our corresponding computed solution in the right column. Note that our computed solution correctly predicts the expansion of a denuded zone around the larger islands. The fastest islands to decay are predicted to be the ones which are relatively small and begin near much larger islands. This leaves the larger islands gradually expanding a denuded zone around them as seen in the final image. While our solutions compare favorably qualitatively, we do not yet completely agree on the time elapsed.

There are several causes for discrepancy between the model and the experiment that should be mentioned. First, there is some discrepancy in the transfer of experimental images into a format suitable for our code. As can be seen by the initial numerical configuration, the data is very rough, so some preprocessing of the experimental data may be necessary to get an accurate start. This variation can play a role in the order of dissolution of the

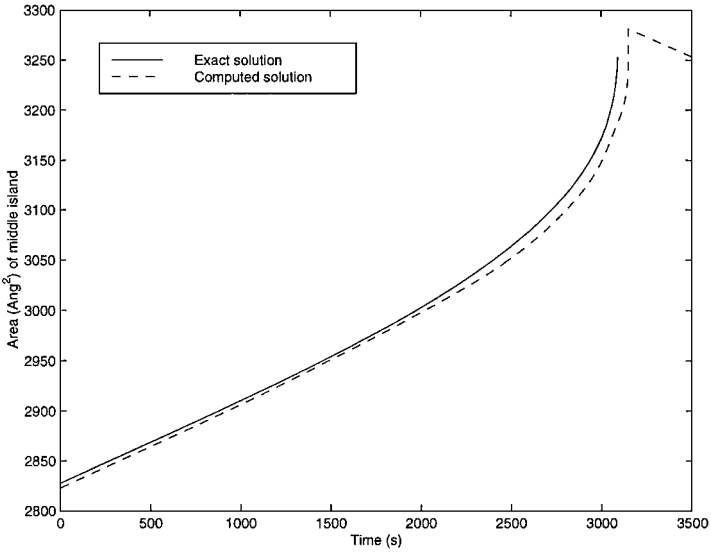

FIG. 9. Plot of full simulation vs ODE solution for middle island.

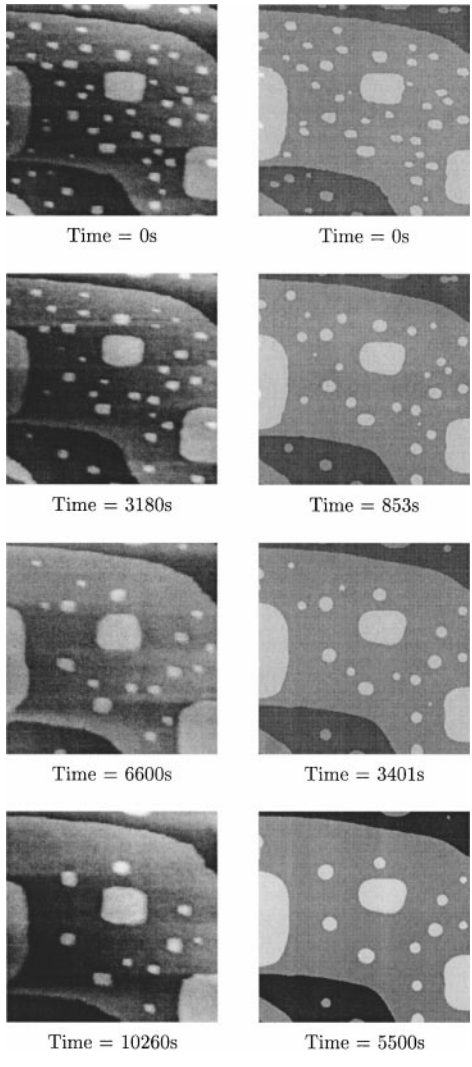

FIG. 10. Time sequence of annealing TiN (002) at 800°C [19] compared with computed solution.

smaller islands, but clearly the selection of the larger islands over longer time scales still holds. Second, we must employ boundary conditions at the sides of the domain which are naturally going to differ from the experimental conditions. Our present algorithm employs zero-flux boundary conditions which tends to preserve islands near the domain boundary longer than they should. We are investigating alternative boundary conditions that will produce more realistic results. Third, we have not yet derived all the correct values for the physical parameters K, D, α, and ρ_∞^{eq}. We plan to use this tool to deduce those parameters for the model by tuning them until we get agreement with experiment.

6. CONCLUSION

In this paper, we have presented an accurate numerical method, which successfully predicts the motion of single atomic layer islands. The method compares very favorably with solutions of model problems and agrees qualitatively with physical experiments. The method has been demonstrated to correctly predict the time of dissolution of islands in model problems while also maintaining very good conservation of mass. This is a tribute to the use of the finite element method to compute the adatom density on the terraces. We have also predicted the correct qualitative behavior of a given experiment. By adjusting parameters to match the physical experiment more accurately, and armed with the results from model problems, we will be able to confidently predict the critical physical constants necessary for any material simulations.

This method also introduces the coupling of level sets with traditional finite element methods. This coupling promises to deliver greater accuracy and reliability into the solution of elliptic equations used in the computation of interface speed functions while still preserving the essential connection of level set methods to the methods from hyperbolic conservation laws.

We will use this method to derive critical physical constants necessary for accurate modeling of a given material. The material we are currently investigating is TiN, but it is clear that this same technique can be applied to a number of different materials to derive basic physical constants. These constants can then be used in various growth models so that accurate predictions about thin-film growth can be made.

ACKNOWLEDGMENT

The author thanks Joe Greene, Suneel Kodambaka, and Patrick Desjardins for very helpful discussions and for providing experimental data with which to work.

REFERENCES

1. D. Adalsteinsson and J. A. Sethian, A unified level set approach to etching, deposition and lithography. I. Algorithms and two-dimensional simulations, *J. Comput. Phys*. **120**, 128–144 (1995).
2. D. Adalsteinsson and J. A. Sethian, A unified level set approach to etching, deposition and lithography. II. Three-dimensional simulations, *J. Comput. Phys*. **122**, 348 (1995).
3. D. Adalsteinsson and J. A. Sethian, A unified level set approach to etching, deposition and lithography. III. Complex simulations and multiple effects, *J. Comput. Phys*. **138**, 193 (1997).
4. D. Adalsteinsson and J. A. Sethian, The fast construction of extension velocities in level set methods, *J. Comput. Phys*. **148**, 2 (1999).
5. M. C. Bartelt, A. K. Schmid, J. W. Evans, and R. Q. Hwang, Island size and environment dependence of adatom capture: Cu/Co islands on Ru(0001), *Phys. Rev. Lett*. **81**(9), 1901 (1998).

6. N. C. Bartelt, W. Theis, and R. M. Tromp, Ostwald ripening of two-dimensional islands on Si(001), *Phys. Rev. B* **54**(16), 11,741 (1996).
7. A. Bogicevic, S. Liu, J. Jacobsen, B. Lundqvist, and H. Metiu, Island migration caused by the motion of the atoms at the border: Size and temperature dependence of the diffusion coefficient, *Phys. Rev. B* **57**(16), R9459 (1998).
8. W. K. Burton, N. Cabrera, and F. C. Frank, The growth of crystals and the equilibrium structure of their surfaces, *Philos. Trans. R. Soc. London A* **243**, 299 (1951).
9. D. L. Chopp, Computing minimal surfaces via level set curvature flow, *J. Comput. Phys*. **106**, 77 (1993).
10. D. L. Chopp and J. A. Sethian, *Flow under Mean Curvature: Singularity Formation and Minimal Surfaces*, Technical Report PAM-541, Center for Pure and Applied Mathematics, University of California, Berkeley, November 1991.
11. G. Ehrlich and F. G. Hudda, Atomic view of surface self-diffusion: Tungsten on tungsten, *J. Chem. Phys.* **44**(3), 1039 (1966).
12. M. Eßer, K. Morgenstern, G. Rosenfeld, and G. Comsa, Dynamics of vacancy island coalescence on Ag(111), *Surf. Sci*. **402**–**404**, 341 (1998).
13. P. Finnie and Y. Homma, Dynamics, interactions, and collisions of atomic steps on Si(111) in sublimation, *Phys. Rev. Lett*. **82**(13), 2737 (1999).
14. M. Giesen and H. Ibach, Step edge barrier controlled decay of multilayer islands on Cu(111), *Surf. Sci*. **431**(1), 109 (1999).
15. G. W. Greenwood, The growth of dispersed precipitates in solutions, *Acta Metallurg.* **4**, 243 (1956).
16. M. F. Gyure, C. Ratsch, B. Merriman, R. E. Caflisch, S. Osher, J. J. Zinck, and D. D. Vvedensky, Level-set methods for the simulation of epitaxial phenomena, *Phys. Rev. E* **58**(6), R6927–R6930 (1998).
17. J. B. Hannon, C. Klünker, M. Giesen, H. Ibach, N. C. Bartelt, and J. C. Hamilton, Surface self-diffusion by vacancy motion: Island ripening on Cu(001), *Phys. Rev. Lett.* **79**(13), 2506 (1997).
18. C. Klünker, J. B. Hannon, M. Giesen, H. Ibach, G. Boisvert, and L. J. Lewis, Activation energy for the decay of two-dimensional islands on Cu(100), *Phys. Rev. B* **58**(12), 7556 (1998).
19. S. Kodambaka, V. Petrova, A. Vailionis, P. Desjardins, I. Petrov, and J. E. Greene, *Time Sequence Images of Annealing TiN(002) at 800°*, Technical Report, University of Illinois Urbana–Champaign, Dept. of Materials Science and Engineering and Matierals Research Laboratory, 1999. [To be published]
20. U. Kürpick, P. Kürpick, and T. S. Rahman, Atomic processes in vacancy island motion on Ag(111), *Surf. Sci*. **383**, L713 (1997).
21. K. Kyuno and G. Ehrlich, Step-edge barriers: Truths and kinetic consequences, *Surf. Sci*. **394**, L179 (1997).
22. I. M. Lifshitz and V. V. Slyozov, The kinetics of precipitation from supersaturated solid solutions, *J. Phys. Chem. Solids* **19**(1/2), 35 (1961).
23. R. Malladi, J. A. Sethian, and B. C. Vemuri, Evolutionary fronts for topology-independent shape modeling and recovery, in *Proceedings of Third European Conference on Computer Vision, Stockholm, Sweden*, volume 800 of *Lecture Notes in Computer Science* Lecture Notes in Computer Science (Springer-Verlag, Berlin/New York, 1994), Vol. 300, p. 3.
24. T. R. Mattsson, G. Mills, and H. Metiu, A new method for simulating the late stages of island coarsening in thin film growth: The role of island diffusion and evaporation, *J. Chem. Phys*. **110**(24), 12,151 (1999).
25. J. G. McLean, B. Krishnamachari, D. R. Peale, Ẽ. Chason, J. P. Sethna, and B. H. Cooper, Decay of isolated surface features driven by the Gibbs–Thompson effect in an analytic model and a simulation, *Phys. Rev. B* **55**(3), 1811 (1997).
26. K. Morgenstern, G. Rosenfeld, and G. Comsa, Decay of two-dimensional Ag islands on Ag(111), *Phys. Rev. Lett*. **76**(12), 2113 (1996).
27. K. Morgenstern, G. Rosenfeld, and G. Comsa, Local correlation during Ostwald ripening of two-dimensional islands on Ag(111), *Surf. Sci*. **441**, 289 (1999).
28. J. J. Mortensen, T. R. Linderoth, K. W. Jacobsen, E. Lægsgaard, I. Stensgaard, and F. Besenbacher, Effects of anisotropic diffusion and finite island sizes in homoepitaxial growth pt on pt(100)-hex, *Surf. Sci*. **400**, 290 (1998).

29. U.S. National Institutes of Health, *NIH Image*, available at http://rsb.info.nih.gov/nih-image.
30. S. Osher and J. A. Sethian, Fronts propagating with curvature-dependent speed: Algorithms based on Hamilton–Jacobi formulations, *J. Comput. Phys.* **79**, 12 (1988).
31. W. W. Pai, A. K. Swan, Z. Zhang, and J. F. Wendelken, Island diffusion and coarsening on metal (100) surfaces, *Phys. Revi. Lett*. **79**(17), 3210 (1997).
32. D. R. Peale and B. H. Cooper, Adsorbate-promoted mass flow on the gold (111) surface observed by scanning tunneling microscopy, *J. Vac. Sci. Technol. A* **10**(4), 2210 (1992).
33. R. L. Schwoebel and E. J. Shipsey, Step motion on crystal surfaces, *J. Appl. Phys*. **37**, 3682 (1966).
34. J. A. Sethian, Curvature and the evolution of fronts, *Commun. Math. Phys*. **101**, 487 (1985).
35. J. A. Sethian, Numerical methods for propagating-fronts, in P. Concus and R. Finn, editors, *Variational Methods for Free Surface Interfaces*, edited by (Springer-Verlag, New York, 1987), p. 155.
36. J. A. Sethian, Numerical algorithms for propagating interfaces: Hamilton–Jacobi equations and conservation laws, *J. Differential Geom*. **31**, 131 (1990).
37. J. A. Sethian, *Level Set Methods: Evolving Interfaces in Geometry, Fluid Mechanics, Computer Vision and Material Science* (Cambridge Univ. Press, Combridge, UK, 1996).
38. J. A. Sethian, A marching level set method for monotonically advancing fronts, *Proc. Nat. Acad. Sci*. **93**(4), 1591 (1996).
39. D. S. Sholl and R. T. Skodje, Diffusion of clusters of atoms and vacancies on surfaces and the dynamics of diffusion-driven coarsening, *Phys. Revi. Lett*. **75**(17), 3158 (1995).
40. C. R. Stoldt, A. M. Cadilhe, M. C. Bartelt, C. J. Jenks, P. A. Thiel, and J. W. Evans, Formation and relaxation of 2D island arrays in metal (100) homoepitaxy, *Prog. Surf. Sci*. **59**(1–4), 67 (1998).
41. G. Strang and G. J. Fix, *An Analysis of the Finite Element Method* (Prentice Hall, New York, 1973).
42. N. Sukumar, D. L. Chopp, N. Moes, and T. Belytschko, Modeling holes and inclusions by level sets in the extended finite element method, submitted for publication.
43. D. J. Trevor and C. E. D. Chidsey, Room temperature surface diffusion mechanisms observed by scanning tunneling microscopy, *J. Vac. Sci. Technol. B* **9**(2), 964 (1991).
44. J. Villain, Healing of a rough surface at low temperature, *Europhys. Lett*. **2**(7), 531 (1986).
45. P. W. Voorhees, The theory of Ostwald ripening, *J. Stat. Phys*. **38**, 231 (1985).
46. J. Zhu and J. A. Sethian, Projection methods coupled to level set interface techniques, *J. Comput. Phys*. **102**(1), 128 (1992).
47. M. Zinke-Allmang, Surface diffusion studies by analysis of cluster growth kinetics, *Scanning Microscopy* **4**(3), 523 (1990).
48. M. Zinke-Allmang, L. C. Feldman, and M. H. Grabow, Clustering on surfaces, *Surf. Sci. Rep*. **16**(8), 377 (1992).